Available online at www.sciencedirect.com

ScienceDirect

Physics Procedia 52 (2014) 36 – 45

Physics Procedia

Physics and Applications of High Brightness Beams Workshop, HBEB 2013

Technology development for short-period magnetic undulators

B.A. Peterson[a], O.D. Oniku[b], W.C. Patterson[b], D. Le Roy[c], A. Garraud[b], F. Herrault[a], N.M. Dempsey[c], D.P. Arnold[b], M.G. Allen[a]

[a]*Georgia Institute of Technology, 791 Atlantic Drive NW, Atlanta, GA 30332, USA*
[b]*University of Florida, Larsen Hall, Gainesville, FL 32611, USA*
[c]*Institut Néel, CNRS-UJF, 25 rue des Martyrs 38042, Grenoble, France*

Abstract

Methods for manufacturing and characterizing permanent-magnet-based short-period undulators are presented. Two fabrication methods, differing by the dimension range of their magnetic period, are described: the mini-undulator, with magnetic periods ranging from 1 mm to 200 µm, fabricated by laser micromachining bulk permanent magnets; and the micro-undulator, with magnetic periods from 200 µm to 10 µm, fabricated by electroplating or sputtering a hard magnetic material onto silicon. The undulator gaps vary from 500 µm down to tens of microns, corresponding to the reduction of the magnetic period. Undulator peak magnetic fields can reach up to 0.7 T while maintaining a reasonable undulator gap. Using these short-period undulators, high-photon-energy radiation can be generated at lower electron beam energies compared to current state-of-the-art undulators.

© 2014 Elsevier B.V. Open access under CC BY-NC-ND license.
Peer-review under responsibility of the scientific committee of HBEB 2013

Keywords: permanent magnet; undulator; micromachining; short-period;

1. Introduction

Magnetic undulators are used in synchrotron sources to create high brightness, narrowband electromagnetic (EM) radiation—typically visible light up to X-ray—by perturbing the trajectory of relativistic electrons [1]. The undulator establishes a spatially varying magnetic field through which the electron beam passes such that the EM radiation propagates on-axis with the electron beam. Undulators generally rely on assemblies of either electromagnets or permanent magnets to generate the periodic magnetic field patterns with peak field intensities in the range of 0.1 – 1.5 T.

An undulator is characterized by the dimensionless undulator parameter:

1875-3892 © 2014 Elsevier B.V. Open access under CC BY-NC-ND license.
Peer-review under responsibility of the scientific committee of HBEB 2013
doi:10.1016/j.phpro.2014.06.007

$$K \cong 0.9337 B_0 [T] \lambda_u [cm] \quad (1)$$

where B_0 is the peak magnetic flux density of the sinusoidally varying magnetic field and λ_u is the spatial period of the magnetic field. For a typical undulator with magnetic field on the order ~1 T and a period of ~1 cm, $K \sim 1$ [2].

The non-dimensional undulator parameter governs the energy bandwidth and brilliance of the resultant radiation [1]. To maximize the spectral purity of the EM radiation, short pole-pitch ($K<<1$) undulators are desired [3]. The fundamental wavelength of the radiation is given by:

$$\lambda_{rad} \cong \frac{\lambda_u}{2\gamma^2}\left(1+\frac{K^2}{2}\right) \approx \frac{\lambda_u}{2\gamma^2} \quad (2)$$

which reduces as shown for $K<<1$, where γ is the Lorentz factor of the relativistic electrons.

A major application area for undulators is generation of soft and hard X-rays. Assuming a conventional undulator with a period of 5 cm, achieving desirable X-ray photon energies (>1 keV) requires electron beam energies in excess of 2 GeV. While such beams exist in large-scale storage-ring and linear accelerator facilities, there is growing interest for more compact and more accessible narrowband X-ray sources. One path to achieve this goal is to shrink the period, λ_u, of the undulator. For example, a 100x reduction in period length (e.g. from 5 cm down to 500 μm) would reduce the required electron beam energy from 2 GeV down to only 200 MeV to produce the same wavelength of radiation.

Alternatively, coupled with high beam energies, miniaturized undulators could conceivably enable generation of even higher-energy monochromatic beams, such as very hard X-rays and even gamma radiation. There is currently strong interest in the medical and scientific communities to generate these higher bands of EM radiation to open new doorways in material science, medical therapy, etc. [4] [5]

Generating higher-energy photons from lower-energy electron beams is naturally attractive, but reducing the undulator period is not without cost. First, reducing λ_u also proportionally reduces K, which results in fewer emitted photons of a higher energy. Both electromagnet and permanent-magnet based undulators are material limited in their maximum magnetic field strength B_0, so there is no obvious way to compensate for this reduction in K. There are also some practical challenges. To maintain sufficient magnetic field strengths, the undulator's air gap (between top and bottom magnet arrays) must also be scaled down proportionally. This narrowed gap demands strict beam alignment and low beam emittances in order to pass the electrons through the structure without beam scraping.

Reduced-pitch undulators based on micromachined electromagnets [6], hybrid permanent micropoles [7], and superconductors [8] have been previously explored. Superconducting approaches are considered more exotic and not further discussed, but of the other two, we argue there are clear advantages to permanent magnets rather than electromagnets in reduced-scale undulators. First, a PM does not require electric power to generate the magnetic field, nor does it require active cooling. Small-scale undulators will generally be placed within the vacuum of the beam-line, so vacuum compatibility and minimization of feed-throughs is a major consideration. Second, permanent magnets can be scaled down and maintain their same field strength, whereas in electromagnets a linear increase in the current density is required as the electromagnet is scaled down [9] [10]. One drawback however is that PM-based undulators have fixed magnetic field strength and period length once assembled. Conventional undulators often require shimming to fine-tune their magnetic field profile [1]; such approaches may be difficult to replicate at small scales.

In this paper, we describe two different manufacturing technologies to enable short-period, permanent-magnet undulators. The focus here is on simple pole arrangements with two poles per period (north-south-north-…) in order to develop and demonstrate the concepts. Herein, "mini" denotes undulators fabricated by top-down laser-micromachining of bulk materials with undulator periods from millimeter length scales down to ~200 μm. We then show methods toward "micro" undulators that employ magnetic films deposited onto silicon substrates, enabling undulator periods from ~200 μm down to potentially below 10 μm.

Nomenclature

PM	permanent magnet
$Co_{80}Pt_{20}$	Cobalt-rich Cobalt-Platinum, permanent magnet material
NdFeB	Neodymium-Iron-Boron, permanent magnet material
SmCo	Samarium-2-Cobalt-17, permanent magnet material

2. Undulator fabrication

In this section, the fabrication approaches for the mini and micro undulators are presented. For mini-undulators, a top-down approach of laser micromachining followed by microassembly is used. For micro-undulators, bottom-up microfabrication techniques—including electroplating and/or sputtering—are used to create magnetic films tens of microns thick followed by selective magnetization to create the magnetic pole patterns. With these two methods of fabrication, it is feasible to create undulators with periods ranging from 1 mm down to below 10 μm.

2.1. Mini-undulator

For the fabrication of a mini-undulator, the first requirement is to use high-energy-product PM materials that are as thin as can be bulk-manufactured and that are also able to withstand the stresses of laser micromachining [11]. The rare-earth substrates used here are bulk pieces of 300-μm-thick samarium-2-cobalt-17 (SmCo). These samples are first laser machined by a Nd:YLF IR laser (Resonetics) with pulse width = 100 μs, pulse period = 1 ms, cut speed = 30 μm/s, with air assist above and vacuum underneath. Using this approach, we have previously demonstrated that the laser micromachined SmCo pieces retain more than 80 % of their magnetization even when machined down to less than 50 μm in width [11]. When cut smaller, the material properties degrade quickly, which is attributed to laser-induced damage. The laser machining hence sets a lower limit for the mini undulator period at about 200 μm.

Using laser-micromachining, the magnets are cut into comb-like structures that can be assembled to form spatially varying magnetic field profiles [12]. The initial laser-machined shape is shown in Figure 1(a). This comb structure is used to help make the undulator design modular (any number of periods) and to provide a backbone that can maintain the desired period. After laser machining, the magnets are cleaned in a citric acid solution (15 % citric acid, at 80 ºC, for 5 min), dipped in an ultrasonic bath, and vapor-coated with a protective 5-μm-thick parylene layer. The comb structures are then magnetized through the thickness direction in a 7 T superconducting magnet (Bruker DSX 300), creating either "north" or "south" arrays. The different comb arrays are eventually assembled as shown in Figure 1(b) with their respective magnetization directions [12]. It should be noted that this arrangement is a favorable placement for the magnetic poles, so the comb arrays easily assemble into these interdigitated structures.

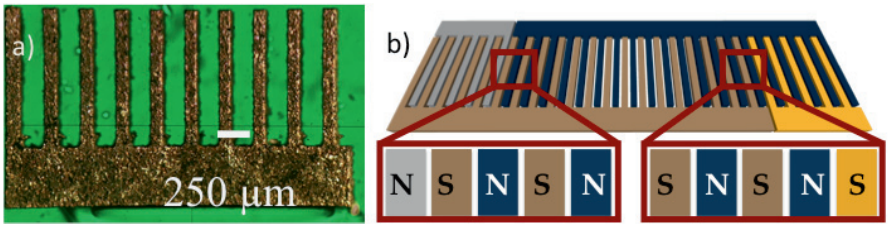

Fig. 1. (a) Top-view photograph of a comb structure after laser micromachining and (b) rendering of an assembled PM array with an alternating magnetic field

The magnet arrays are then placed in a recessed cavity in a non-magnetic frame (aluminum in this case) and adhered to it using vacuum-safe epoxy(e.g. Varian TorrSeal); this frame provides the mechanical bracketing for eventual external assembly. The magnets and frame are then polished using a rock slide polishing tool with sandpaper and polishing papers, see Figure 2(b). To maintain a known gap, we laser machine shims from non-magnetic (copper in this case) shim stock. An assembled undulator thus comprises two frames, each housing a magnet array, which are fastened together but separated by two copper shims—one on each long edge of the magnet arrays. The region between the two facing magnet arrays is the gap through which the electron beam will pass. For beamline experiments, the undulator is then placed into an adapter allowing for precise alignment of the 2–mm–wide by 0.2–mm–tall gap with any electron beam or magnetic field measurement device. Figure 2 shows a photograph of a fully assembled undulator in an adapter along with the top view of a single frame bearing a 400–µm–period magnet array. The array comprises fifty magnet pole pairs.

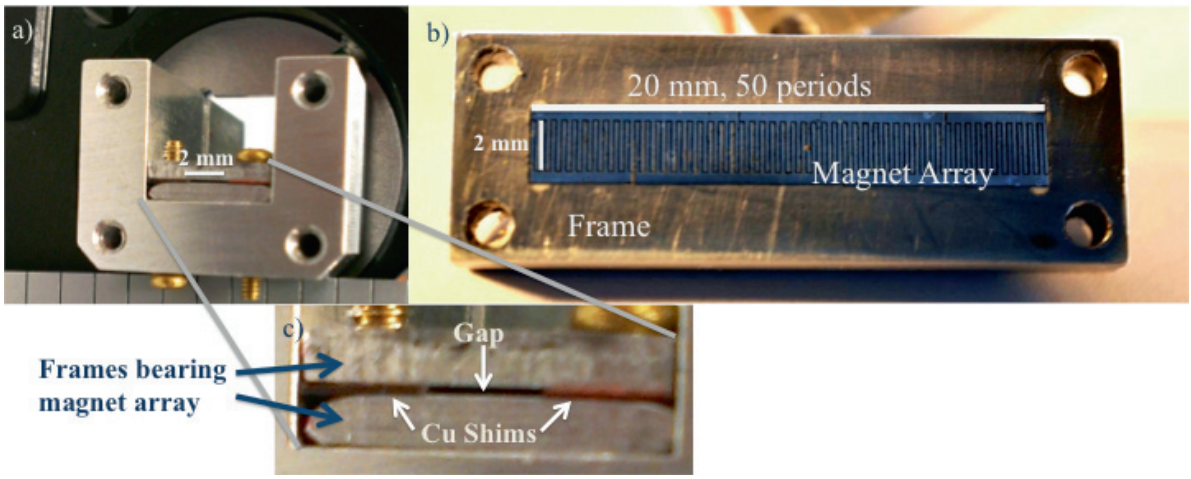

Fig. 2. (a) Photograph of the front of an assembled undulator in an adapter; (b) Top-view photograph of a magnet array (another magnet array placed directly above creates an undulator); and (c) Zoomed front-view photograph of the assembled undulator with frames and shims visible.

2.2. Micro-undulator

For the development of the micro-undulator, the initial task is to fabricate PM films that will subsequently be magnetized to obtain the alternating magnetic poles of the undulator. In this work, two different materials are considered: electroplated Co-rich Co-Pt films and sputtered NdFeB. In brief, the Co-rich Co-Pt ($Co_{80}Pt_{20}$) films are electroplated onto Cu seed layers on silicon substrates using the processes described in [13]. Under the right

deposition conditions, these films exhibit a strong magnetocrystalline anisotropy in the as-deposited state, without any post-deposition temperature treatment. The NdFeB films are sputtered at 400 °C onto silicon substrates using the process discussed in [14]. Films of 100-nm-thick tantalum are used as adhesion buffer and capping layers. A post-deposition annealing treatment at 750 °C for 10 min is needed to crystallize the hard magnetic phase, so as to achieve high values of coercivity. The demagnetization curves of these films—measured by vibrating sample magnetometer—are shown in Figure 3 for a 15-µm-thick electroplated $Co_{80}Pt_{20}$ and a 5-µm-thick sputtered NdFeB film. They present a coercivity of 200 kA/m and 840 kA/m and a remanence of 0.58 T and 1.3 T, respectively.

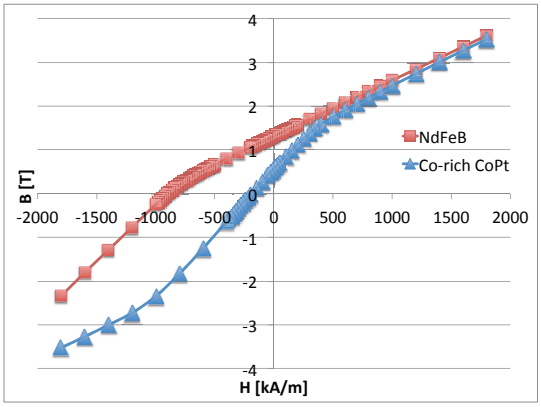

Fig. 3. Demagnetization curves (B vs. H) for Co-rich Co-Pt, and NdFeB.

A selective magnetization process [15] is then used to obtain the alternating magnetic pole patterns necessary for use in an undulator. Figure 4 shows the procedure used for magnetic patterning of these thin films. The magnetic layer is first pre-magnetized to induce a magnetization in the north direction through the thickness of the entire layer. A micromachined soft-magnetic magnetizing head is then brought in contact with the magnetized layer. In this case, a 125–µm–thick iron (Fe) sheet is cut using a 355–nm wavelength laser to form the magnetizing head (Oxford Lasers). The soft magnetizing head is composed of a periodic array of 2-mm-long rectangular slits with slit widths ranging from 100 µm down to 30 µm. Figure 5 shows the top view of the three magnetizing heads used in this work.

With the magnetizing head in place, a pulsed magnetic field is applied in the reverse direction as shown in Figure 4(c). Due to the high magnetic saturation magnetization (~2.1 T) and high relative permeability of iron ($\mu_r \approx$ 4,000), the regions that are in direct contact with the magnetizing head (covered regions in the figure) experience a stronger reversal field than the uncovered regions, thus inducing a south pole in the covered regions. A pattern of alternating poles (north-south-north-…) is thus produced in the hard magnetic film; this forms the magnet array for the micro-undulator. As in the mini-undulator case, to form a complete undulator, two identical magnet arrays would be assembled with a gap set by spacer shims. Shims for the micro-undulator can be machined and placed or deposited via microfabrication on the silicon substrate itself.

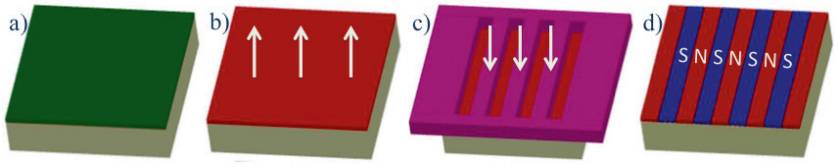

Fig. 4. Fabrication process: (a) Begin with unmagnetized electroplated $Co_{80}Pt_{20}$ or sputtered NdFeB film; (b) Magnetize the film; (c) Bring film in contact with magnetizing head and apply a reversal field; (d) Magnetic patterns are formed based on the features of the magnetizing head.

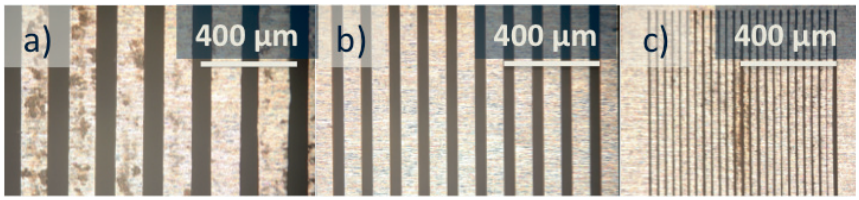

Fig. 5. Top view of Fe magnetizing heads for (a) 200–µm–period, (b) 120–µm–period, and (c) 65–µm–period magnetic patterns.

3. Magnet array characterization

Due to the small spatial size of the magnetic field patterns of these mini- and micro-undulators, characterization of the magnetic fields presents significant challenges. Multiple methods exist for measuring fully assembled large-scale undulators including pulsed-, vibrating-, and moving-wire systems, as well as Hall-effect sensor probes [1]. For mini- and micro-undulators we have successfully used a scanning Hall-effect sensor and magneto-optical imaging over a single open-faced magnet array. Characterizing the magnetic fields in the narrow gap of a completely assembled mini or micro undulator remains an open challenge.

3.1. Scanning Hall probe system

Hall-effect sensors have long been used to measure the magnetic flux density inside undulators. Most commercial Hall probes are based on sensors which have dimensions on the order of, or larger than, mini-undulator period lengths. This causes averaging to occur over the width of the sensor active area. As such, for measurement of mini- and micro-undulators, more specialized high-resolution Hall sensors are required with active sensing areas smaller than a single pole width (i.e., 1 µm – 10 µm).

Scanning the Hall probe over a magnet array provides a detailed view of the magnetic flux density over a single magnet array. Due to the size of the mini- and micro- undulators, the sensor must also be in close proximity (< 200 µm) to the surface of the magnets and is only capable of sensing the field perpendicular to the plane. Figure 6 shows Hall probe measurements taken ~80 µm above the surface of four magnet arrays with differing period lengths (λ_u = 400 µm, 300 µm, 250 µm, and 230 µm). Due to superposition of magnetic fields, the on-axis field in an ideal undulator (two vertically stacked, identical arrays) would be approximately double the field strength of a Hall probe measurement over a single array. Using this fact and simulations of the magnetic fields (presented in the next section), we are able to predict, with reasonable accuracy, the field within a mini- or micro- undulator.

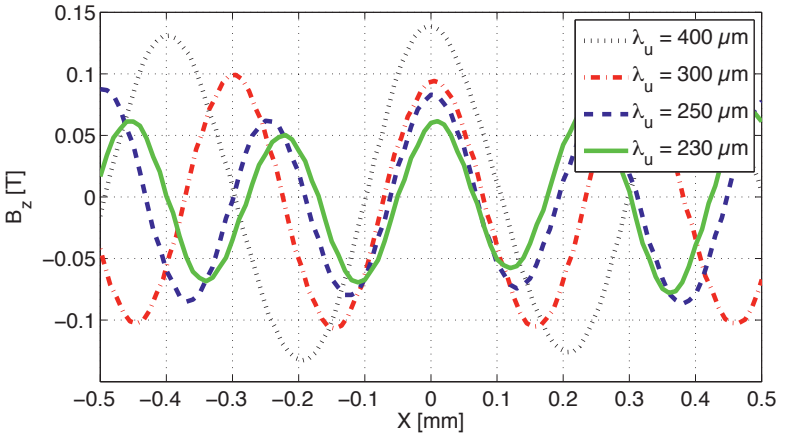

Fig. 6. Magnetic flux density measurements from a scanning Hall-effect sensor taken ~80 μm above the surface of four, laser-machined "mini" magnet arrays (period lengths of 400 μm, 300 μm, 250 μm, and 230 μm) along what would be the undulator axis as a function distance.

The measurement results, taken using the Hall-effect sensor over an open magnet face, are then compared with a finite-element simulation (COMSOL Multiphysics) of the predicted fields. Figure 7 shows a comparison of the magnetic fields from a measured magnet array and a COMSOL Multiphysics simulation, indicating good agreement.

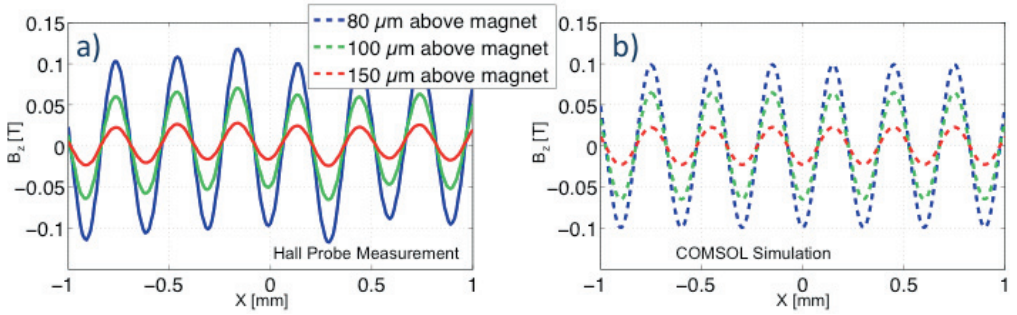

Fig. 7. Magnetic field measurements (a) and respective COMSOL simulations (b) along the centerline of a 300-μm-period magnet array at various heights (80, 100 and 150 μm) from the surface of the magnet.

3.2. Magneto-optical imaging film

As a complement to the scanning Hall probe magnetic field measurements, magneto-optical indicator films (MOIF) are used to provide a qualitative image of the stray field pattern produced by the magnet arrays. Placing a MOIF layer in contact with the surface of a magnetic array facilitates a microscopic optical image of the magnetic fields by using a microscope with a polarized illumination and a polarization analyzer. It functions by using the Faraday effect, which describes how the polarization of light rotates as it passes through a magnetic material [16]. The uniaxial MOIF used here, which is made of bismuth-substituted yttrium iron garnet (Bi:YIG), which has a high Faraday rotation coefficient, reveals the direction of the z-component of the stray field produced by the magnet array upon which it is positioned. Such a MOIF provides a spatial resolution of about 10 μm. The possibility of using MOIF for quantitative imaging of the field patterns produced by micron-scaled magnets is also

being explored. This may be necessary for measuring the magnetic fields from the $Co_{80}Pt_{20}$ and NdFeB thin films, because the current scanning Hall probe measurements are too far from the surface of the thin films, whereas the height at which the MOIF measures the magnetic field is its thickness (~1 µm).

The MOIF is used to reveal the magnetic field pattern (north or south) produced by the magnet arrays of period lengths 200 µm, 120 µm, and 65 µm. Figure 8 shows the magnetic field patterns obtained by selective magnetization of both the $Co_{80}Pt_{20}$ and the NdFeB thin films. The patterns in the $Co_{80}Pt_{20}$ films are obtained using a reversal magnetic field of 0.5 T, whereas the patterns in the NdFeB films require a reversal field of 1.5 T due to the higher coercivity of the NdFeB film (840 kA/m, compared to 200 kA/m for $Co_{80}Pt_{20}$). Note that the areas outside the selectively magnetized regions do not present enough magnetic fields to saturate the MOIF, and hence show the natural, labyrinth-like domain structure of the YIG layer.

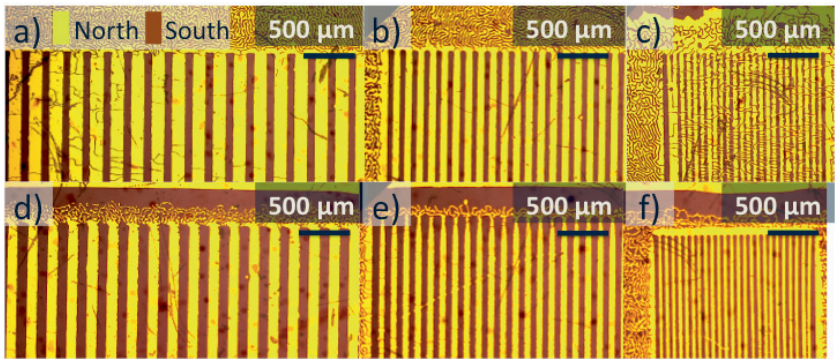

Fig. 8. MOIF images of a (a & d) 200–µm–period, (b & e) 120–µm–period, and (c & f) 65–µm–period magnetic pattern on (a-c) a 15–µm–thick electroplated Co-rich CoPt film and (d-f) a 5–µm–thick sputtered NdFeB film.

4. Undulator simulations

As mentioned previously, simulations provide a check for our Hall probe measurements, but can also be useful for designing new geometries and modifying our undulator to produce specific EM radiation spectra. Thus, finite-element simulations (COMSOL Multiphysics) are additionally used to simulate the B-field produced by a micro-undulator modeled in 2D, having 50 periods. The arrays are designed with a 15–µm–thick hard magnetic film with a 50–µm period, north and south poles having the same width. The simulation is performed with gaps ranging from 10 µm to 50 µm, with the nominal gap value being 20 µm for the 15–µm–thick film. The two hard magnetic materials considered for the simulation are $Co_{80}Pt_{20}$ and NdFeB.

The undulator properties expected from using these two materials are listed in Table 1 along with mini-undulator properties for comparison. The B-field expected on-axis for the undulator made from the NdFeB film is about four times stronger than the B-field of the undulator made from $Co_{80}Pt_{20}$. Figure 9 shows the on-axis peak B-field from the 50–µm–period NdFeB undulator as a function of undulator gap size.

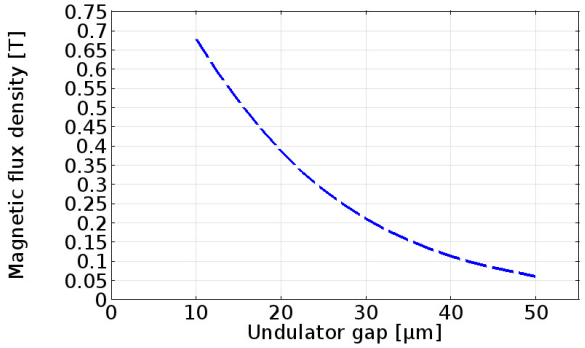

Fig. 9. Simulated peak on-axis B-field from the NdFeB undulator as a function of gap size.

Table 1: Summary of mini- and micro-undulator designs.

Undulator magnetic material	Gap (μm)	PM thickness (μm)	Period (μm)	B-field (T) (peak, on-axis)	K
Laser machined SmCo	200	200	400	0.23	0.0086
Plated Co-rich Co-Pt	20	15	50	0.101	0.00047
Sputtered NdFeB	20	15	50	0.386	0.00180

5. Summary

We have shown the feasibility of fabrication for miniature undulators with period lengths from 1 mm down to tens of microns with at least one complete undulator prototype at a period length of 400 μm. These undulators will allow for future linear accelerators to be smaller and more portable, for a given desired output energy, leading to greater efficiency and accessibility throughout the medical and scientific communities. Future developments include the characterization and testing of these undulator structures in photon-generation experiments. Also, more complex magnetic arrangements with correspondingly higher magnetic field levels are envisioned in future work.

Acknowledgements

This work was supported by the DARPA AXiS program under grant #N6601-11-1-4198.

References

[1] J. Clarke, *The Science and Technology of Undulators and Wigglers*.: Oxford University Press, 2004.

[2] D. Attwood, *Soft X-Rays and Extreme Ultraviolet Radiation: Principles and Applications*.: Cambridge University Press, 1999.

[3] G. Brown, K. Halback, J. Harris, and H. Winick, "Wiggler and Undulator Magnets - A Review," *Nuclear Instruments and Methods*, vol. 208, pp. 65-77, 1983.

[4] T.S. Lawrence, R.K. Ten Haken, and A. Giaccia, "Principles of Radiation Oncology," in *Cancer: Principles and Practices of Oncology*, 8th ed., V.T. Jr. DeVita, T.S. Lawrence, and S.A. Rosenberg, Eds. Philadelphia: Lippincott Williams and Wilkins, 2008.

[5] G.S. Was, *Fundamentals of Radiation Materials Science: Metals and Alloys*.: Springer, 2007.

[6] J. Harrison, A. Joshi, J. Lake, and R. Candler, "Surface-micromachined magnetic undulator with period length between 10 μm and 1 mm for advanced light sources," *Phys. Rev. ST Accel. Beams*, vol. 15, no. 7, p. 070703, 2012.

[7] R. Tatchyn et al., "Generation of Soft X-Ray/VUV Photons with a Hybrid/Bias Micropole Undulator on the LLNL Linac," *Journal of X-Ray Science and Technology*, vol. 1, no. 1, pp. 79-98, 1989.

[8] T. Hezel et al., "A superconductive undulator with a period length of 3.8 mm," *J. Synchrotron Radiat*, vol. 5, pp. 448-450, 1998.

[9] "Specialized Course on Magnets," in *CERN Accelerator School*, Bruges, Belgium, 2009, p. 494.

[10] O. Cugat, J. Delamare, and G. Reyne, "Magnetic Micro-Actuators and Systems (MAGMAS)," *IEEE Transactions on Magnetics*, vol. 39, no. 5, pp. 3607-3612, Nov 2003.

[11] B. A. Peterson et al., "Assessment of Laser-Induced Damage in Laser-Micromachined Rare-Earth Permanent Magnets," *IEEE Transactions on Magnetics*, vol. 48, no. 11, pp. 3606-3609, 2012.

[12] B. A. Peterson, W. C. Patterson, F. Herrault, D. P. Arnold, and M. G. Allen, "Laser-micromachined permanent magnet arrays with spatially alternating magnetic field distribution," in *PowerMEMS*, Atlanta, 2012, pp. 319-322.

[13] O. D. Oniku and D. P. Arnold, "Microfabrication of High Performance Thick Co80Pt20 Permanent Magnets for Microsystems Applications," *ECS Transactions*, vol. 50, no. 10, pp. 167-174, 2013.

[14] N. M. Dempsey et al., "High performance hard magnetic NdFeB thick films for integration into micro-electro-mechanical systems," *Applied Physics Letter*, vol. 90, p. 092509, 2007.

[15] O. D. Oniku, R. Regojo, Z. A. Kaufman, W. C. Patterson, and D. P. Arnold, "Batch patterning of sub-millimeter features in hard magnetic films using pulsed magnetic fields and soft magnetizing heads," *IEEE Transactions on Magnetics*, vol. In Press, 2013.

[16] R.M. Grechishkin, S. Chigirinsky, M. Gusev, O. Cugat, and N.M. Dempsey, *Magnetic Nanostructures in Modern Technology*, B. Azzerboni et al., Eds. Dordrecht: Springer-Kluwer Academic, 2007.